Annealing of multivacancy defects in 4*H*-SiC

W. E. Carlos,* N. Y. Garces, and E. R. Glaser
Naval Research Laboratory, Washington, D.C. 20375, USA

M. A. Fanton
Electro-Optics Center, Pennsylvania State University, Freeport, Pennsylvania 16229, USA
(Received 14 July 2006; revised manuscript received 29 September 2006; published 1 December 2006)

The annealing behavior of defects observed in electron paramagnetic resonance (EPR) and photoluminescence (PL) is discussed. We consider the divacancy (the P6/P7 EPR centers) and a previously unreported EPR center that we suggest is a V_C-V_{Si}-V_C trivacancy and their relationship with each other and with the UD1–3 series of PL lines near 1 eV. We observe that the divacancy and the UD2 PL lines annealing behavior is strongly correlated further establishing the relationship between the EPR and PL centers. We present a detailed discussion of this center and its ^{29}Si and ^{13}C hyperfine spectra which supports our assignment as a trivacancy. The intensity of this center increases with annealing temperature as the divacancy decreases and there is a sample-to-sample correspondence between the overall intensities of the two centers. However, the details of their annealing suggest a more complex relationship than a simple one-to-one transformation. In addition, while the UD1 PL increases with annealing temperature, sample-to-sample variations indicate it is not related to this EPR center.

DOI: 10.1103/PhysRevB.74.235201 PACS number(s): 78.40.Fy, 61.72.Hh, 78.55.−m

As wide band gap semiconductor technology based on the III-nitrides and SiC matures, the performance of high power microwave devices based on these materials are surpassing traditional Si technology.[1] The 4*H* polytype of SiC has emerged as an especially important material for such electronics because of its availability, high electron mobility, large band gap, and high thermal conductivity. Point and extended lattice defects play a crucial role in these materials both in limiting performance and in compensating shallow dopants in semi-insulating (SI) substrates.[2,3] Structural identification of such defects is important to understand the formation of these defects and to limit or optimize their concentration. A number of native defects such as the isolated vacancies, the divacancy, and the carbon vacancy-carbon antisite pair have been identified by electron paramagnetic resonance (EPR).[4] Although the identity of the defect or defects responsible for the SI behavior or limiting device performance has not been determined, it is becoming increasingly apparent that more than one defect and more complex defects may be crucial to understanding the compensation mechanism in SI substrates or in limiting properties such as carrier lifetime.

There have been a number of experimental and theoretical studies of the annealing and stability of fundamental defects in SiC.[5–9] Much of the experimental work has been on irradiated material where a primary process is the recombination of vacancies and interstitials. In as-grown material there are few interstitials and so such processes are much less important. In such material the C vacancy is less mobile than the Si vacancy with the former being stable to 1600–1700 °C (Ref. 7) while we find the V_{Si} anneals at ~1200 °C. As we show later, the divacancy is also quite stable to ~1500–1600 °C.

In this work, we discuss the annealing behavior of the divacancy and its relationship to the UD2 PL lines. In addition we focus on a defect (denoted ANN1) that may be related to the divacancy and which we identify as a trivacancy (V_C-V_{Si}-V_C) complex. This may be one of the simplest of a family of more complex defects that play a role in the SI character of these substrates and the starting point of vacancy clusters which would develop into more extended defects. EPR work has also been reported on larger less well-defined clusters of vacancies.[10]

I. EXPERIMENT

The samples used in this work are standard commercially available physical vapor transport (PVT) or high temperature chemical vapor deposition (HTCVD) grown SI substrates with *B* and *N* levels below 10^{16} cm^{-3} (Ref. 2). Details of sample characteristics before annealing are given in Table I. All samples were annealed for 30 min in an argon atmosphere with an estimated cool down time of ~30 min, which

TABLE I. The growth techniques and initial characteristics of the sample sets used in this study.

Sample	Growth Technique	Initial Characteristics	Initial Resistivity
A	PVT	Strong Si Vac., Weak *C* Vac.	1×10^{6} Ω cm
B	PVT	No Si Vac., Strong *C* Vac.	5×10^{11} Ω cm
C	HTCVD	No Si Vac., Strong *C* Vac., Strong UD1 PL	1×10^{11} Ω cm
D	PVT	SI5(V_C-C_{Si}) EPR	5×10^{11} Ω cm

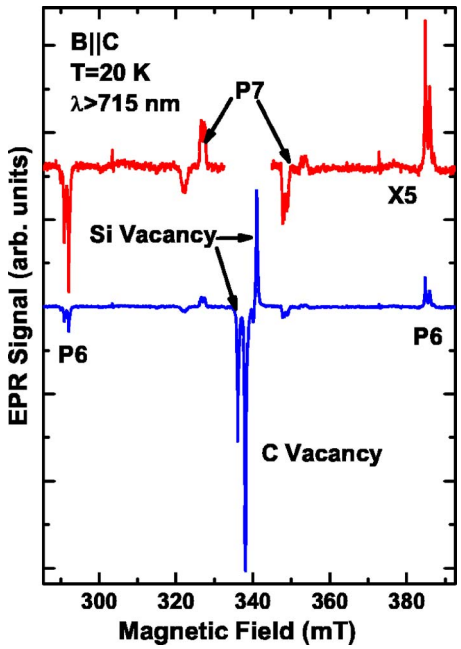

FIG. 1. (Color online) A representative EPR spectrum illustrating the P6/P7 centers (the divacancy) in an unannealed sample. Also shown are the isolated vacancies.

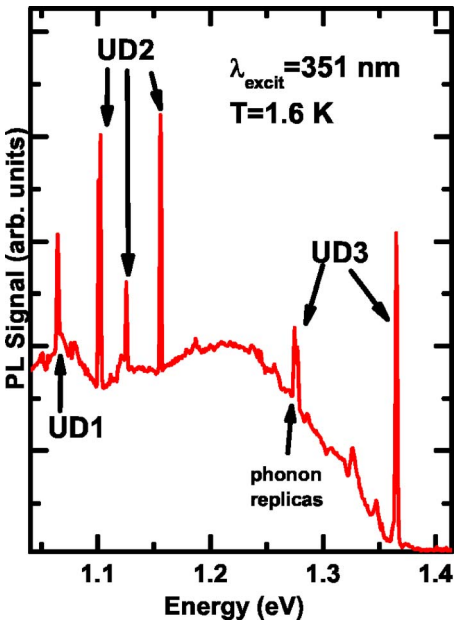

FIG. 2. (Color online) The photoluminescence (PL) spectrum illustrating the UD1, UD2, and UD3 IR PL lines.

is much more rapid than typical cooling rates in bulk growth, possibly quenching in metastable defects. All EPR/PL samples for different anneal temperatures from a given wafer were adjoining pieces cut from near the wafer center. At the higher temperatures, the annealing resulted in visible graphitization of the surfaces. The thin graphite layer was removed by annealing in an oxygen atmosphere at 1000 °C for approximately one h. Electrical measurements on sister pieces annealed at the same temperatures (but a different time) showed steady decreases in the room temperature resistivities with annealing from $\sim 10^6 - 10^{12}$ ohm·cm to 10–1000 ohm·cm.[11]

The EPR spectra were obtained using a conventional 9.5 GHz spectrometer equipped with a liquid helium flow system for temperature control with optimal data obtained between 10 and 100 K. The EPR studies required rapid passage conditions[12] and/or optical excitation. Either a xenon lamp and various filters or an Ar^+ laser through an optical fiber provided the required optical excitation. Both absorption in quadrature with the magnetic field modulation and dispersion measurements were used. The former gives a derivative line shape and better resolution while the latter gives a stronger undifferentiated signal. Relative intensities were obtained by double or single integration of the respective line shapes. Considerable care was taken to maintain the same optical intensity from run to run and results were quite reproducible. The PL measurements on the same pieces used for EPR were performed at 1.6 K. The emission was excited by the 351-nm line of an Ar^+ laser, analyzed by a 1/4-m double-grating spectrometer, and detected by a liquid nitrogen-cooled Ge photodiode.

II. RESULTS

The divacancy, first observed by Vainer and Il'in in irradiated 6H-SiC (Ref. 13) is commonly seen in SI substrates and has been associated with the P6/P7 EPR centers[14–16] and these in turn, have been linked with the UD2 IR PL between 1.1 and 1.16 eV.[17] Magnusson and Janzén have recently argued that the P6/P7 centers are associated with a different set of PL lines between 1.0 and 1.06 eV.[18] This second set of lines does line up reasonably well with the MCD (magnetic circular dichroism) detected absorption lines which have been associated with the P6/P7 EPR lines by Lingner *et al.*[19] However, this second set of lines is only seen in lightly *n*-type materials while UD2 and P6/P7 are common to SI material. It is quite possible that both sets of lines are related to the divacancy but in somewhat different configurations. Here, we briefly restate our original arguments and provide further data in support of the coupling of UD2 and P6/P7. In Fig. 1 we show a representative P6/P7 EPR spectrum. The P6 lines have axial C_{3V} symmetry and the accepted model is a V_C-V_{Si} divacancy oriented along the *c* axis.[14] The P7 lines have C_{1h} symmetry and are due to a divacancy oriented along a basal bond direction. In Fig. 2 we show representative IR PL spectra to illustrate the UD1-3 lines commonly seen in these substrates. Of particular interest are the UD2 lines which we have previously associated with the P6/P7 EPR centers. Previously we have shown that the P6 centers have sharp zero phonon lines (ZPL) near 1.1 eV in photo-EPR and that these match up with two of the four UD2 lines. The P7 lines do not have sharp ZPL in photo-EPR but their onset does match up reasonably well with the other two lines in the UD2 PL spectrum. In this work we discuss the annealing behavior of the P6 centers and their corresponding UD2 lines, shown for two samples in Fig. 3. It is perhaps not too surprising that as the anneal temperature increases both the EPR and the PL spectral intensities decrease. However, note that a number of details of the annealing behavior of the P6 lines are reflected in that of the UD2 PL lines. In all samples there is rapid decrease in both EPR and PL between 1400 and 1600 °C; however, in sample D both the PL and EPR

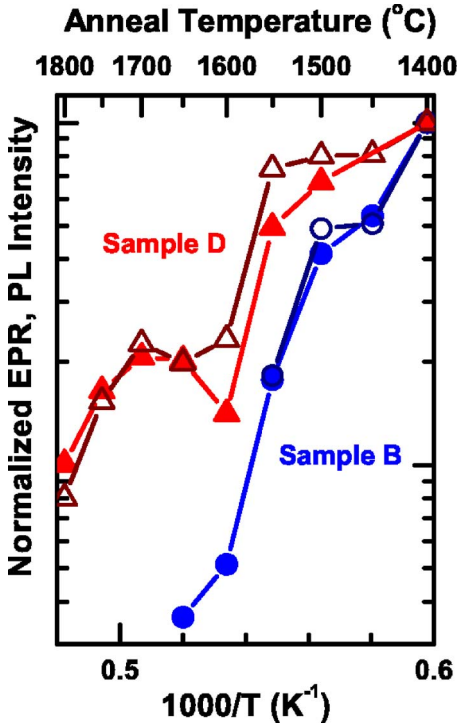

FIG. 3. (Color online) The P6 EPR (closed symbols) and 1.1 eV doublet of the UD2 IR PL (open symbols) intensities as a function of anneal temperature. The intensities are normalized to the values of sample *D* at 1400 °C.

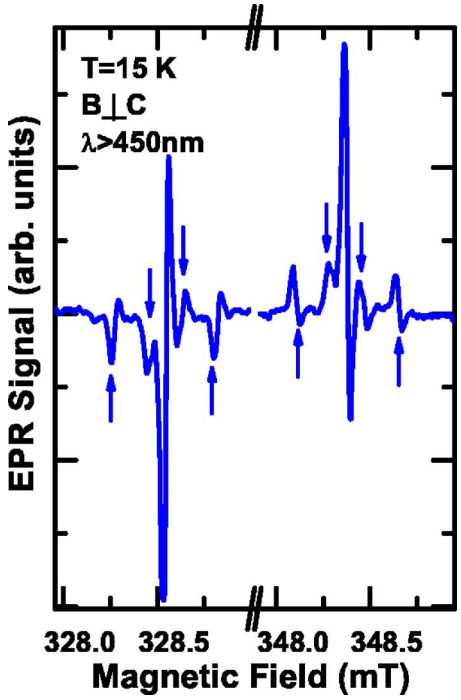

FIG. 4. (Color online) The EPR spectrum of the ANN1 center. The up arrows indicate the $A=15.4$ MHz ^{29}Si hyperfine satellites and the down arrows indicate the $A=4.2$ MHz ^{29}Si hyperfine satellites.

level off and decrease only very slowly between 1600 and 1800 °C while in sample B the signals drop to zero. While it is possible to propose a number of models to account for this apparent two step behavior, the fact that the PL mimics the EPR as well as it does can only be explained by both being due to the same structural defect. Also, we observe that the slope of the PL and EPR intensities vs 1/T is very similar, especially in sample B ($E_A \sim 7$ eV) where the annealing behavior is rather simple. Finally, we remark that sample-to-sample correlations between not only the overall intensities but also relative peak intensities support the association of the UD2 PL and the P6/P7 EPR. In summary, the annealing behavior, the optical response, and sample-to-sample variations all support the identification of the UD2 PL as arising from the P6/P7 EPR centers which have been convincingly associated with the divacancy.

In Fig. 4, we show the spectrum of a defect whose parentage may be the divacancy. No signal is seen in the dark—this may be because this defect is diamagnetic in the ground state but can be optically excited into a paramagnetic $S=1$ triplet state. It could also be that the ground state is the triplet and optical excitation serves to increase the population of the $m_S=0$ state and take the spin system out of thermal equilibrium greatly enhancing the intensity of the EPR lines. It has been shown that this is true with other defects in SiC.[14,20] In either case, the phase of one of the sets of lines (the low field in this case) are inverted because the center is being optically pumped, resulting in the $m_S=0$ level being almost completely filled and the $m_S=\pm 1$ levels being nearly empty.[21] Hence, the low field lines are due to stimulated emission while the high field lines are due to absorption, similar to that shown for the P6/P7 centers in Fig. 1.

The angular dependence of this spectrum is shown in Fig. 5 for rotations about the $[11\bar{2}0]$ and [0001] directions. For an arbitrary direction of the magnetic field, there are three magnetically inequivalent, but crystallographically equivalent sites of the defect in the SiC lattice. When the external magnetic field is restricted to a $\{11\bar{2}0\}$ plane, the spectrum consists of two lines, one of which is doubly degenerate; this degeneracy is removed if the magnetic field is out of the plane. For rotations in the (0001) plane, the spectrum splits into three components. Along the *c* axis all the sites are degenerate and only one pair of lines is observed. The points in Fig. 5 are the experimental data and the solid lines are generated using best fit parameters obtained by exact diagonalization of the matrix form of the following spin-Hamiltonian (Ref. 22):

$$\hat{H} = g\beta \mathrm{SB} + D\left[S_z^2 - \frac{1}{3}S(S+1)\right] + E\left[S_x^2 - S_y^2\right], \qquad (1)$$

where β is the Bohr magneton, B the magnetic field, and D and E are the axially symmetric component and the asymmetry parameter of the crystal field interaction, respectively. This results in $g=2.0056$ (isotropic); $D=-279.8$ MHz; $E=5.6$ MHz. Clearly the principal axis of the crystal field interaction is along a $\langle 1\bar{1}00\rangle$ direction. It might seem unusual that the crystal field term is nearly axial even though the principal axis is in the basal plane. However, the P7 defect (the divacancy oriented along a basal bond direction) has a

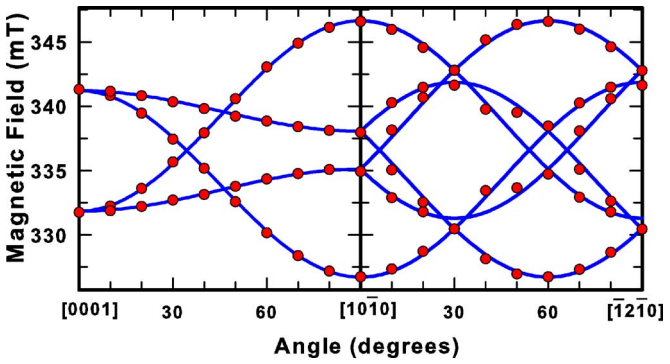

FIG. 5. (Color online) The orientation dependence of the ANN1 center for rotations about a $\langle 11\bar{2}0\rangle$ axis on the left and about the [0001] axis on the right. The positions of the resonances are indicated by the solid circles and the lines are a fit to a Hamiltonian containing Zeeman and crystal field terms.

range of $|E/D|$ values from 0.2% for one site in 6*H* SiC (Ref. 19) to 20% for one site in 4*H* (Ref. 15) and so the ratio of ~2% in this case does not seem unreasonable. This may indicate that the defect wave function is highly localized and not very sensitive to the surrounding lattice. Two ^{29}Si hyperfine values were also measured, $A=15.4$ MHz and 4.2 MHz, each due to between two and four ^{29}Si nuclei. The orientation of the defect suggests a pair of like nearest-neighbor vacancies while the intensities of the Si hyperfine interactions suggest a pair of *C* vacancies. The ^{29}Si hyperfine splittings are isotropic to within experimental accuracy and quite small indicating that only a small portion (<10%) of the defect wave function is localized on those atoms. In Fig. 6, we show a simulation of the hyperfine structure around the high field line assuming the 4.2 MHz interaction is due to four Si neighbors and the 15.4 MHz interaction is due to two Si neighbors. In addition to the primary hyperfine lines, there are weaker lines, as indicated by the arrows in Fig. 6 that are due to two ^{29}Si atoms around the center. In particular, notice the very weak lines at about 333.0 and 334.1 mT in the simulation. These are due to two ^{29}Si atoms on the two 15.4 MHz sites and are too weak to be observed above other small signals in the data. Other possible configurations involving three or four atoms on these sites result in much stronger lines at these positions which would be visible above the background. For instance, if there were an equal number of sites with both the 4.2 and 15.4 MHz hyperfine interaction these two outer lines would have the same intensity as the other hyperfine lines due to two ^{29}Si atoms. Such lines would clearly be above the background: the fact that they are not supports the model with only two atoms with this hyperfine interaction. In Fig. 7 we show the ^{13}C hyperfine structure that we believe is due to two carbon atoms which are nearest neighbors, along with the two C vacancies, to a central Si vacancy. For $B\|[1\bar{1}00]$ the hyperfine interaction is 84.2 MHz and the intensity of these two lines is ~1.6% of the total, consistent with two C neighbors. By symmetry, the hyperfine interaction due to the two C atoms should be degenerate for $B\|[1\bar{1}00]$ and should broaden and then split for angles away from this orientation. In Fig. 7 we

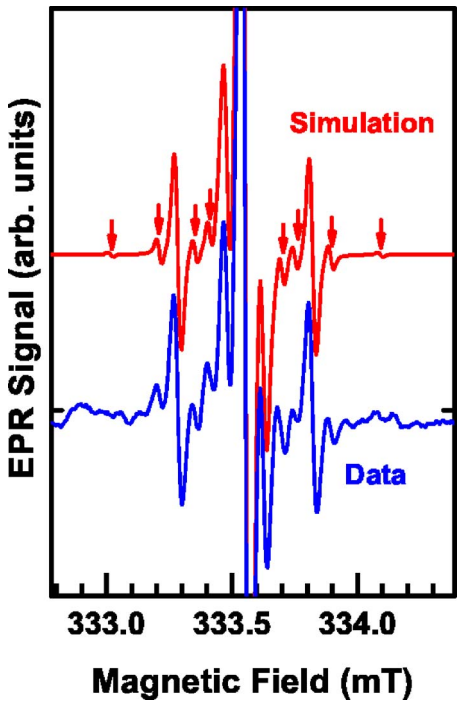

FIG. 6. (Color online) A comparison of the EPR spectrum of the low field ANN1 line and a simulation assuming two Si nearest neighbors with a hyperfine interaction of 15.4 MHz and four with a hyperfine interaction of 4.2 MHz. The arrows indicate hyperfine lines due to two ^{29}Si neighbors.

observe the hyperfine structure does split for small rotations; although the resolution is not as good as one would like. The individual hyperfine lines appear to broaden somewhat and there is interference from other weak resonances making a full rotation study infeasible. The principal part of the wave function is on these two atoms. Assuming all sp^3 wave functions, a simple atomic orbital calculation yields: 10% on each of the two C atoms, 0.5% on each of four Si atoms, and 1.6% on each of two Si atoms. If the carbon atoms relax away from the Si vacancy, their wave functions will be less *s*-like and the calculated concentrations larger and the data in Fig. 7 suggests significant anisotropy (e.g., for only a 10° rotation the two pairs give interactions of 74.1 MHz and 87.7 MHz vs 82.7 MHz and 85.9 MHz expected for an sp^3 orbital) but we have been unable to obtain sufficient angular dependence to accurately determine the full ^{13}C hyperfine tensor. These calculations are quite simplistic and do not take into account effects such as spin polarization which can be quite significant.[23]

We originally proposed that this center could be due to two carbon vacancies around a carbon antisite:[24] however, the splitting of the hyperfine spectra described above indicates that two C atoms are involved and we are not able to resolve any other ^{13}C hyperfine lines that might be attributable to a single central atom. We can also rule out a Si atom on this site, since the hyperfine lines from a single ^{29}Si atom would be roughly twice as intense as seen for the two ^{13}C atoms. One other possibility is an impurity atom with no isotope of significant abundance (>1 at %) with a nuclear spin; e.g., oxygen. Lacking evidence to the contrary, we

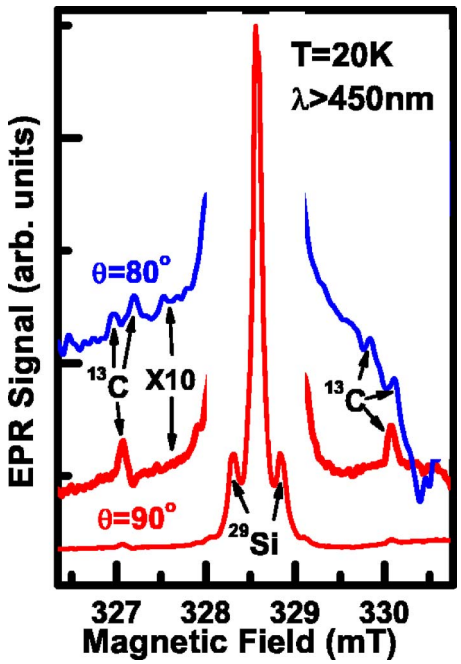

FIG. 7. (Color online) The ^{13}C hyperfine interaction satellites around the low field EPR line of the ANN1. The angles are with respect to the *C* axis. The $\theta=80°$ spectrum has been shifted by about 1.15 mT so that the central portions of the spectrum are approximately aligned. (Only the 15.4 MHz ^{29}Si hyperfine lines are resolved, the 4.2 MHz lines are obscured by the central line.)

adopt a provisional model of the defect as V_C-V_{Si}-V_C.

There are two possible atomic configurations which could, in principle, fit the data. In the first, the two carbon vacancies lie in the basal plane and the two remaining carbon atoms lie in a $\{1\bar{1}00\}$ plane. In the second configuration, the roles are reversed and the two vacancies lie in a $\{1\bar{1}00\}$ plane and the remaining carbon atoms are in the basal plane. The latter is preferred since the spin is primarily on the two atoms in the basal plane aligned along a $\langle 1\bar{1}00\rangle$ direction which accounts for the symmetry of the crystal field term. We assume that the observed ^{29}Si hyperfine interactions are due to the six Si atoms bonded to the principal pair of carbon atoms. Naturally other assignments are quite plausible and theoretical calculations will be needed to sort out the detailed assignments. The atomic structure of these configurations is shown in the "ball and stick" pictures in Fig. 8 with the principal Si and C atoms labeled (a), (b), and (c). Interestingly, we only observe a signal from the one configuration, suggesting that the configuration with the carbon vacancies in a $\{1\bar{1}00\}$ plane and the other two C atoms in the basal plane has a significantly lower formation energy. Furthermore, we do not see separate signals due to different combinations of hexagonal and cubic sites. This is consistent with the wave function being on the two C atoms in the basal plane with weak interactions with surrounding planes.

We briefly summarize the evidence for the V_C-V_{Si}-V_C model for this center. (i) The symmetry of the crystal field indicates two like atom sites. (ii) The intensity of the ^{29}Si hyperfine interactions points to a pair of carbon vacancies.

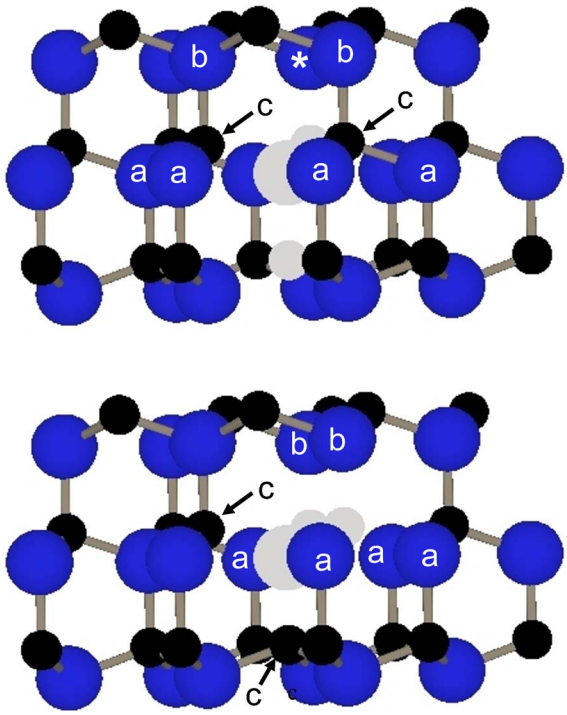

FIG. 8. (Color online) Models showing possible configurations of the trivacancy. The model on top with the two carbon vacancies in a $\{1\bar{1}00\}$ plane is preferred over the one on the bottom with the two vacancies in the basal plane as discussed in the text. The larger balls represent Si atoms and the smaller ones C atoms with light gray balls representing the vacancies. The (a) Si atoms have the 4.2 MHz hyperfine interaction, the (b) Si atoms have the 15.4 MHz hyperfine interaction, and the two C atoms marked with (c) have the principal ^{13}C hyperfine interaction. The Si site marked with an asterisk may be the C antisite as discussed in the text.

(iii) The ^{13}C hyperfine interaction indicates two carbon atoms are involved around the central Si site between the two V_C's. (iv) There is no hyperfine interaction due to the central site which is most probably a silicon vacancy. As discussed in the previous paragraph, the two carbon vacancies are in a $\{1\bar{1}00\}$ plane, while the other two carbon atoms around the V_{Si} lie in the basal plane.

The EPR intensity of this center increases significantly with annealing in all samples as well as showing considerable dependence on the starting material, as shown in Fig. 9. We note that samples *B* and *D* have the strongest overall signals and also have the largest divacancy signals in the unannealed samples suggesting some relationship between the divacancy and ANN1. The V_C-V_{Si}-V_C defect could result from the capture of a C vacancy or quite possibly a Si vacancy by a divacancy. While the capture of a C vacancy is straightforward, the mechanism involving the Si vacancy requires a little explanation. If a Si vacancy moves to a next-nearest-neighbor position to the Si site of the divacancy, the C atom between the two defects could move into the Si vacancy leaving behind a C vacancy and creating a C antisite. This is similar to the mechanism proposed by Lingner and co-workers for the annealing of the isolated Si vacancy.[19] The intensity of the divacancy decreases with an-

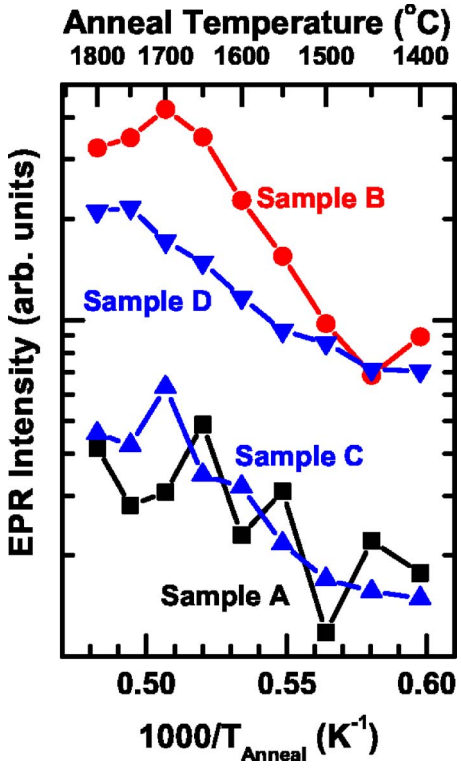

FIG. 9. (Color online) The intensities of the ANN1 EPR signal as a function of anneal temperature for the four samples as indicated.

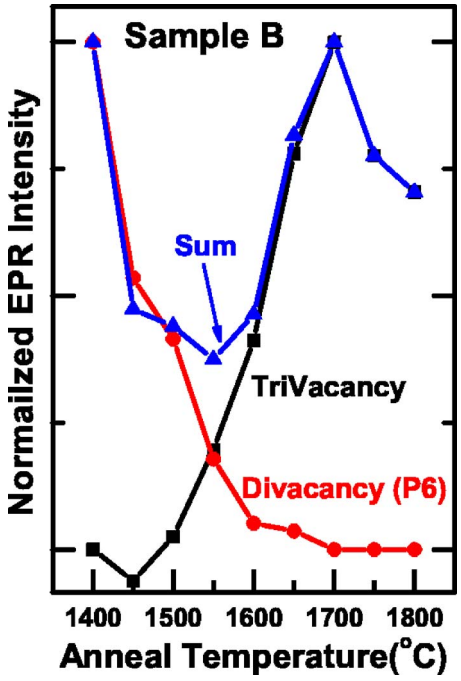

FIG. 10. (Color online) The normalized intensities of the divacancy and ANN1 signals and their sum for sample *B*. The divacancy is normalized to its value at $T_A = 1400$ °C and ANN1 to its value at $T_A = 1800$ °C. Similar results are observed for other samples.

nealing as that of the V_C-V_{Si}-V_C defect increases, although there is not a one-to-one correspondence. If it were a simple conversion of the divacancy to a trivacancy, the sum of the two intensities would be roughly a constant. As we see illustrated for sample *B* in Fig. 10 this is hardly the case and furthermore we see that the concentration of the divacancy decreases sharply before that of ANN1 begins to increase and has dropped below the detection limit while the ANN1 signal continues to increase. The ANN1 signal decreases after higher temperature, presumably due to conversion to another defect which we are not able to detect in EPR. Similar results are observed for the other samples. Previous reports have shown the concentration of carbon vacancies does not change appreciably with annealing up to 1700 °C while the Si vacancy becomes mobile at ~1200 °C. While we do not detect the Si vacancy after these anneal temperatures, only the negatively charged state has been identified; although, the positive and neutral states are thought to be in the gap and paramagnetic. One might speculate that the process is something like:

$$V_C - V_{Si} + V_{Si} \rightarrow V_C - V_{Si} - C - V_{Si} \rightarrow V_C - V_{Si} - V_C - C_{Si} \quad (2)$$

in which the intermediate structure, V_C-V_{Si}-C-V_{Si}, is diamagnetic or, at least, not observed in our EPR measurements. The *C* antisite would be reasonably removed from the principal atoms in the defect wave function as shown in Fig. 8 and should relax away from the vacancy. Therefore, it should have little effect on the EPR signal. This would account for the minimum in the sum of the divacancy and ANN1 EPR signals around $T_A \approx 1550$ °C as shown in Fig. 10.

The IR PL was monitored as a function of anneal temperature. The UD1 PL signal as shown in Fig. 11 increases with anneal temperature while the UD2 and UD3 PL signals decrease. A cursory look at Figs. 9 and 11 might suggest a relationship between UD1 and the ANN1 EPR center. However, while both the UD1 PL line and the ANN1 EPR center increase more or less monotonically with anneal temperature, UD1 increases by a factor of about 8 vs a factor of about 3 for the EPR. Furthermore, there is little correlation between samples (e.g., sample *C* has the strongest PL signal and one of the weaker EPR signals, while samples *B* and *D* have strong EPR and weak UD1 PL.) It seems more likely that UD1 and UD3 are inversely related, although we do not have a good model for either. This is illustrated in Fig. 12 in which we plot the sum of the intensities of the UD1 and UD3 PL signals normalized to their values after 1800 °C and 1400 °C anneals, respectively. The three PVT samples (*A*, *B*, and *D*) give a sum which has a standard deviation of 9–13% about the mean. The HTCVD sample (*C*) follows a somewhat different behavior, perhaps because it is grown at a very different temperature. We see in Fig. 11 that the intensity of UD3 in sample *C* increases until it reaches a maximum after the 1550 °C anneal. (UD3 decreases monotonically with anneal temperature in the other three samples.) If we replot Fig. 12 in which the UD3 signal has been normalized to its value after the 1550 °C anneal, the sum is then relatively constant

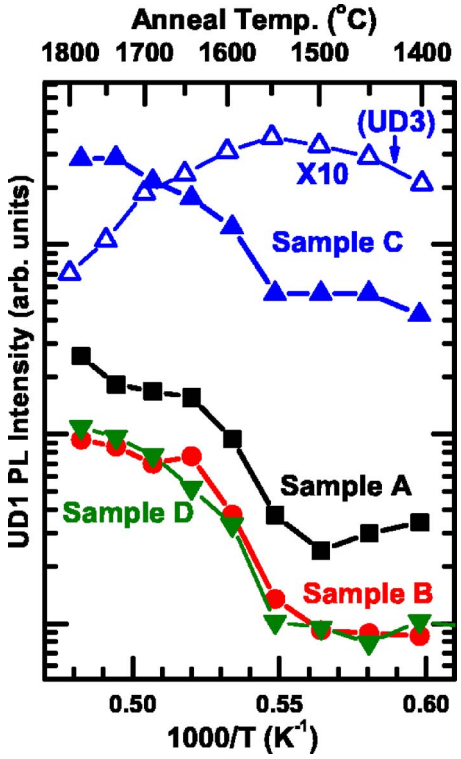

FIG. 11. (Color online) The intensities of the UD1 PL as a function of anneal temperature for the four samples as indicated. Note the correspondence between symbols and samples is the same as in Fig. 9 (e.g., sample *A* is squares and so forth.)

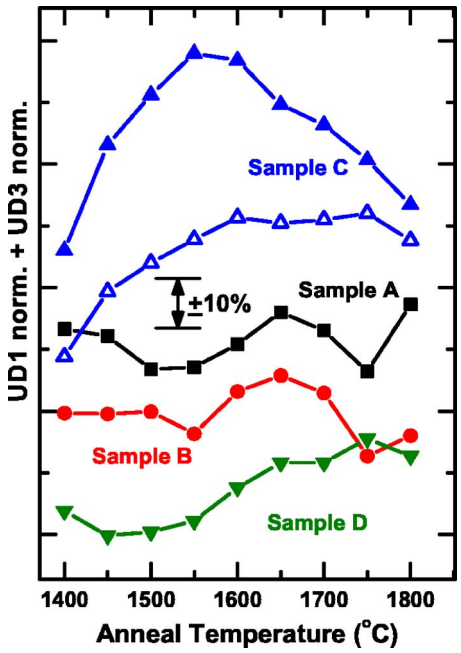

FIG. 12. (Color online) The sum of the UD1 PL normalized to its value after an 1800 °C anneal and the UD3 PL normalized to its value after a 1400 °C anneal as a function of anneal temperature. Data for samples *A*, *B*, and *D* have been offset for clarity. The arrow indicates ±10% deviation from the mean. Also included is the data in which the UD3 PL for sample *C* (the HTCVD sample) were normalized to its value after a 1550 °C anneal (open triangles). Note the correspondence between symbols and samples is the same as in previous figures (e.g., sample *A* is squares and so forth.)

between 1550 °C and 1800 °C anneals. Both UD1 and UD3 change by about an order of magnitude with annealing while their sum changes by only about ±10%, suggesting they are related. Magnusson and co-workers[18] have argued that these centers may be due to impurities and their inverse relationship might further argue that they are due to the same impurity; e.g., in different charge states.

III. SUMMARY

High temperature anneals were used to study the evolution of native defects in semi-insulating, ultrahigh purity 4H SiC. We present additional evidence to support the assignment of the UD2 PL lines to the P6/P7 EPR lines, which are due to the divacancy. The UD2 PL has very similar annealing behavior to that of the divacancy, even mimicking a two step behavior seen in some samples. We also see that sample-to-sample variations are consistent with the relationship and previous work had shown that the zero phonon absorption lines of the P6 center observed in photo-EPR aligned with the emission line observed in PL. We observe a defect that we preliminarily identify as the V_C-V_{Si}-V_C trivacancy based on the symmetry of the crystal field term and the ^{29}Si and ^{13}C hyperfine interactions. The largest hyperfine interaction is with the two C atoms next to the Si vacancy. Based on the symmetry of the crystal field splitting we believe these C atoms are in a basal plane while the three vacancies lie in a $\{1\bar{1}00\}$ plane. The intensity of this center increases with annealing temperature for all sample sets and is strongest in samples that had the strongest initial divacancy signals. It is proposed that the divacancy anneals by capturing an isolated vacancy (either C or Si). However, a simple capture mechanism would imply a one-to-one correspondence between the divacancy and the trivacancy. Since this is not observed, we suggest an intermediate diamagnetic species which would account for the minimum in the combined EPR signal around 1550 °C. The UD1 defect observed in IR PL also increases with annealing; however, neither a sample-to-sample comparison nor the details of the annealing behavior of the EPR center and UD1 support a relationship between UD1 and ANN1. For instance, the samples with the strongest ANN1 EPR signal (*B* and *D*) have weak UD1 PL while the sample with the largest PL (*C*) has a weak EPR signal. Our results are consistent with a relationship between the UD1 and UD3 PL signals which indicate that both are due to the same impurity or lattice defect.

ACKNOWLEDGMENTS

Work at NRL was supported by work at Penn State was supported by AFRL and ONR. N.Y. Garces was financially supported by the National Research Council. We thank Sung Wook Huh of Carnegie Mellon University for the resistivity measurements.

*Electronic address: Carlos@Bloch.NRL.Navy.Mil

[1] For a recent reviews see; S. Sriram, A. Ward, J. Henning, and S. T. Allen, MRS Bull. **30**, 308 (2005); R. C. Clarke and John W. Palmour, Proc. IEEE **90**, 987 (2002).
[2] J. R. Jenny, St. G. Müller, A. Powell, V. F. Tsvetkov, H. M. Hobgood, R. C. Glass, and C. H. Carter, Jr., J. Electron. Mater. **31**, 366 (2002).
[3] Ellison, B. Magnusson, C. Hemmingsson, W. Magnusson, T. Iakimov, L. Storasta, A. Henry, N. H. Henelius, and E. Janzén, Mater. Res. Soc. Symp. Proc. **640**, H1.21.1 (2001).
[4] For a recent review see N. T. Son, Mater Res. Soc. Symp. (to be published).
[5] C. C. Ling, C. D. Beling, and S. Fung, Phys. Rev. B **62**, 8016 (2000).
[6] H. J. von Bardeleben, J. L. Cantin, I. Vickridge, and G. Battistig, Phys. Rev. B **62**, 10126 (2000).
[7] D. Alvarez, V. V. Konovalov, and M. E. Zvanut, J. Electron. Mater. **32**, 444 (2003).
[8] Z. Zolnai, N. T. Son, C. Halin, and E. Janzén, J. Appl. Phys. **96**, 2406 (2004).
[9] E. Rauls, Th. Frauenheim, A. Gali, and P. Déak, Phys. Rev. B **68**, 155208 (2003).
[10] I. V. Ilyin, M. V. Muzafarova, E. N. Mokhov, P. G. Baranov, S. B. Orlinskii, and J. Schmidt, Physica B **340-342**, 128 (2003).
[11] Sung Wook Huh, A. Y. Polyakov, and M. Skowronski (unpublished).
[12] A. M. Portis, Phys. Rev. **91**, 1071 (1953); M. Weger, Bell Syst. Tech. J. **39**, 1013 (1960).
[13] V. S. Vainer and V. A. Il'in, Sov. Phys. Solid State **23**, 2126 (1981).
[14] P. G. Baranov, I. V. Il'in, E. N. Mokhov, M. V. Muzafarova, S. B. Orlinskii, and J. Schmidt, JETP Lett. **82**, 441 (2005).
[15] N. T. Son, P. Carlsson, J. ul Hassan, E. Janzén, T. Umeda, J. Isoya, A. Gali, M. Bockstedte, N. Morishita, T. Ohshima, and H. Itoh, Phys. Rev. Lett. **96**, 055501 (2006).
[16] We note that there has been some controversy over whether the P6/P7 EPR centers are associated with the divacancy or the V_C-C_{Si} pair defect. The work in Refs. 14 and 15 has resolved this in favor of the divacancy.
[17] W. E. Carlos, E. R. Glaser, and B. V. Shanabrook, Physica B **340-342**, 151 (2003); Mater. Sci. Forum **457-460**, 461 (2004).
[18] B. Magnusson and E. Janzén, Mater. Sci. Forum **483-485**, 341 (2005).
[19] Th. Lingner, S. Greulich-Weber, J.-M. Spaeth, U. Gerstmann, E. Rauls, Z. Hajnal, Th. Frauenheim, and H. Overhof, Phys. Rev. B **64**, 245212 (2001).
[20] S. B. Orlinski, J. Schmidt, E. N. Mokhov, and P. G. Baranov, Phys. Rev. B **67**, 125207 (2003).
[21] D. H. Tanimoto, W. M. Ziniker, and J. O. Kemp, Phys. Rev. Lett. **14**, 645 (1965).
[22] See, for example, W. Low, *Paramagnetic Resonance in Solids* (Academic Press, NY, 1960) p. 46.
[23] M. Cook and C. T. White, Phys. Rev. B **38**, 9674 (1988).
[24] W. E. Carlos, N. Y. Garces, E. R. Glaser, and B. V. Shanabrook, Mater. Sci. Forum **527-529**, 531 (2006).